Soft Matter

PAPER

Cite this: *Soft Matter*, 2021, **17**, 9353

Multilobular morphology: the key for biphase multifunctional nanogels†

A. S. Sonzogni,[a] S. Hamzehlou,[b] V. D. G. Gonzalez,[a] J. R. Leiza[b] and R. J. Minari*[a]

Received 30th June 2021,
Accepted 15th September 2021

DOI: 10.1039/d1sm00968k

rsc.li/soft-matter-journal

Nanogels play a leading role in controlled release systems because they possess high water retention capacity resulting in high loading capabilities, stability in biological fluids and biocompatibility. In this scenario, every tool that allows extending the nanogel properties and expanding their potential applications is of high interest in the field of biomedicine. This article aims to contribute to the development of multifunctional nanogels, based on the combination of two polymer phases in a multilobular morphology. The synthesized multilobed nanogels (mLNGs) presented a core of crosslinked poly(*N*-vinylcaprolactam) (PVCL) and a shell formed by 3-D distributed lobes of a low T_g copolymer. This particular multilobular morphology is able to exploit the synergetic contribution of both phases. While the PVCL-based core conferred its characteristic thermal response and the ability to load and release a cargo molecule, the low T_g lobes incorporated the capability of film formation. Moreover, the multilobular arrangement of NGs allows films to undergo unrestricted mass transfer. The development of mLNG morphology and the effect of synthesis parameters were deeply studied with the help of a previously developed mathematical model for the dynamic evolution of particle morphology. Finally, this study presents, for the first time, the synthesis of two-phase nanogels with multilobular morphology and underlines their potential as a candidate for controlled delivery platforms.

Introduction

Nanogels (NGs) play a leading role in biomedical applications, representing a powerful tool to improve the current therapy and diagnostic techniques.[1] These crosslinked nanoparticles have very attractive properties such as high water retention capacity, easy preparation, controllable size, high drug and bio-molecule loading capacity, high stability in biological fluids, *etc.* In addition, depending on their composition, they are able to respond to different stimuli such as pH, temperature, ionic strength and electric field.[2]

Among stimuli responsive NGs, temperature-sensitive ones have aroused high interest because of their potential in controlled delivery of therapeutics.[3–7] Poly(*N*-vinylcaprolactam) (PVCL) is an attractive NG building block because it presents a higher biocompatibility compared to other thermoresponsive polymers[8] and PVCL NGs experiment a swell-collapse transition close to the human physiological temperature.[9] The synthesis of PVCL NGs and their application in controlled delivery of different therapeutics were extensively studied.[4,5,10–13] Due to their great potential and design flexibility, the applications of PVCL NGs have been rapidly extended by adding inorganic compounds[14] or different functionalities for promoting the pH[15] and redox responses.[16,17] However, the synthesis of two-phase polymer–polymer NGs with expanded functionalities has not been exploited. The addition of a second polymeric phase in NGs could be the key for fabricating advanced nano-delivery platforms as a result of the synergetic effect.[18,19]

The success of NGs in controlled release is related to their large exposed surface area and the good mass transfer between their crosslinked structure and the medium. These features allow NGs to load and release different types of molecules. The presence of a second phase should not restrict or alter the mass transfer of cargo molecules. Therefore, in this work, the synthesis of biphase PVCL NGs with multilobular morphology is proposed (Fig. 1). These multilobed NGs (mLNGs) exhibit a multifunctional performance such as thermoresponsiveness, loading and releasing a cargo molecule, and the film formation ability due to the synergetic contribution of both phases. The crosslinked PVCL core helps in maintaining a free interface in contact with the medium, where the transfer of a therapeutic molecule and its thermal controlled shrinking and swelling ability are not

[a] *Group of Polymers and Polymerization Reactors, INTEC (Universidad Nacional del Litoral-CONICET), Güemes 3450, Santa Fe 3000, Argentina. E-mail: rjminari@santafe-conicet.gov.ar; Tel: +54-0342-4558450*

[b] *POLYMAT, Kimika Aplikatua saila, Kimika Fakultatea, University of the Basque Country UPV/EHU, Joxe Mari Korta Zentroa, Tolosa Hiribidea 72, 20018, Donostia/San Sebastián, Spain*

† Electronic supplementary information (ESI) available. See DOI: 10.1039/d1sm00968k

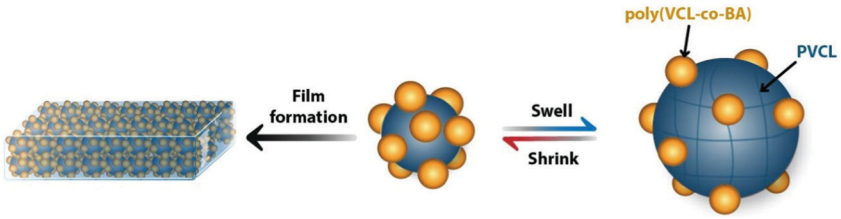

Fig. 1 Schematic morphology of biphase mLNGs.

restricted. On the other hand, the shell formed by 3-D distributed lobes, which is based on a low transition temperature copolymer (containing butyl acrylate, BA, and *N*-vinylcaprolaptam, VCL), confers the last sought task, film formation. It is worth mentioning that to have a multifunctional performance the multilobular morphology should be maintained at the film forming temperature. The presence of VCL in the composition of the lobes is required for compatibilizing both phases. These mLNGs were synthesized by a one-pot semibatch emulsion polymerization strategy. Two mLNGs with different average numbers of lobes per NGs were synthesized, and a mathematical model[20] recently developed for the prediction of the dynamic morphology evolution of composite particles was used to study the effect of reaction parameters on the final morphology. mLNGs could be potentially used as protein dermal-delivery platforms, since they combine the high local hydration of NGs and the occlusion phenomenon of films. This combination of properties can lead to the weakening of the stratum corneum, facilitating the penetration of macromolecules such as proteins.[21] This work reveals for the first time the synthesis of biphase NGs with a multilobular morphology, which is the key promoter of this synergetic multifunctional functionality.

Materials and methods

Materials

N-Vinylcaprolactam (VCL, 98% purity, Aldrich) and butyl acrylate (BA, 99% purity, Aldrich) were used as monomers and *N*,*N*-methylenebisacrylamide (BIS, 99.9% purity, Genbiotech) was used as a crosslinking agent. The employed initiator was potassium persulfate (KPS, 99% purity, Mallinckrodt). Other reagents were sodium bicarbonate ($NaHCO_3$, 99.7% purity, Cicarelli) as buffer, sodium dodecyl sulphate (SDS, Anedra) as an emulsifier, and hydroquinone as a polymerization inhibitor (99% purity, Fluka AG). Deuterated water and sodium acetate (NaAc, 99% purity, Cicarelli) were used as the solvent and internal standard for ^{1}H NMR measurements, respectively. All reagents were used as received without any kind of purification. Distilled and deionized water was used throughout the work.

Polymerization

A one-pot semibatch emulsion polymerization process was designed to reach slower and controlled growth of PVCL NGs and to achieve efficient incorporation of BA in the particle shell. The polymerization process is summarized in Table 1. The reaction temperature was 70 °C and polymerization was carried out under continuous N_2 bubbling. The polymerization set-up involves a 200 mL-jacketed glass reactor equipped with an automatic feeding system, mechanical stirring, a steam condenser, sampling output, N_2 inlet, a digital thermometer, and a thermostatic bath.

Table 1 General procedure for mLNGs synthesis with a reaction volume of 270 mL

Reagent	Total mass (g)
VCL	12
BIS	0.48
BA	8
SDS	0.52
KPS	0.2
$NaHCO_3$	0.2

Fig. 2 presents a sketch of the semibatch synthesis strategy with the monomer dosing profiles distributed in a timeline. The total amount of VCL was split into two equal parts, one half as an initial load and the other half is dosed along the polymerization. Hence, synthesis started with an aqueous emulsion containing the initial load of VCL, SDS, $NaHCO_3$, and BIS. After reaching the reaction temperature, a KPS solution was injected to initiate the polymerization. At this time, the dosing of pre-emulsion containing the remaining VCL, SDS, and $NaHCO_3$ was started at a constant feed rate until t_F^{dos} time (Scheme A). During VCL dosing, an aqueous pre-emulsion of BA was fed in a separated stream from t_{BA}^{dos} until t_F^{dos} times (Scheme B). Once the feeding period was over, the polymerization conditions were maintained for an additional 30 min (Scheme C). Two mLNGs (mLNGs-1 and mLNGs-2) were synthesized with this strategy with the dosing parameters presented in Table 2. Detailed procedures, involving the mass amount per stream could be found in Table S1, ESI.†

Film formation

Films were prepared by casting the dialyzed mLNG dispersions into silicon molds at room temperature in a desiccator with silica gel until achieving a constant weight. The final thickness of dry films was about 1 mm.

Characterization

Monomer conversion and average particle diameter were measured on the withdrawn samples along both reactions. Monomer conversion was measured by ^{1}H NMR spectroscopy following the method reported elsewhere for VCL.[11] The spectra

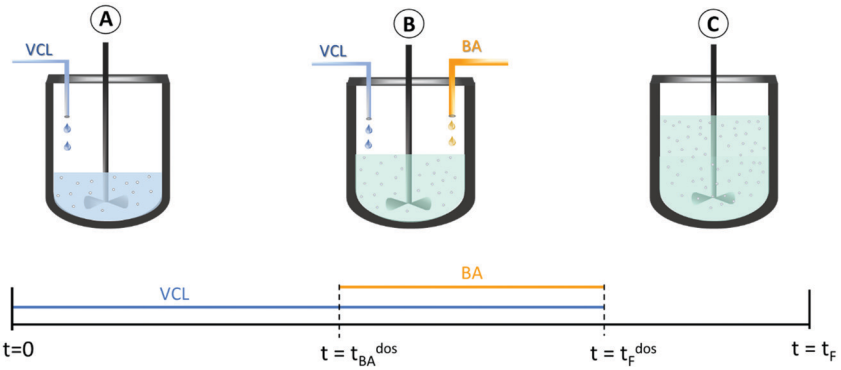

Fig. 2 Scheme of the semibatch polymerization set-up and monomer loading profiles during the reaction.

Table 2 Dosing parameters for the synthesis of mLNGs-1 and mLNGs-2

Experiment	VCL mass flow rate [g min^{-1}]	BA mass flow rate [g min^{-1}]	t_{BA}^{dos} [min]	t_F^{dos} [min]	t_F [min]
mLNGs-1	1.18	0.60	50	90	120
mLNGs-2	0.30	0.15	200	360	390

were recorded with a Bruker advance II 300 MHz spectrometer using a Watergate technique (83919GP, relaxation time (D1):1.00 s) to remove the water signal. Monomer conversion was calculated on the basis of the peak areas corresponding to the vinyl bond and the internal standard (AcNa).

The average particle diameter (D) of NGs was determined by dynamic light scattering (DLS) at a detection angle of 90°, in a Brookhaven BI-9000 AT photometer. The thermal response of final NGs was also determined by measuring D by DLS of dilute samples (1 mg mL^{-1}) at increasing temperatures (from 20 °C up to 55 °C, with 20 min of stabilization).

Differential scanning calorimetry analysis (DSC) was performed using a TA Instruments (DSCQ2000) system. Dried latex samples of 5–7 mg were analyzed using a sealed aluminum pan (TZero technology). DSC measurements were carried out from −90 to 300 °C with a heating rate of 10 °C min^{-1}. The results obtained during the first heating cycle are reported as a derivative from heat flow (dDSC), while those of the second heating cycle can be found in the ESI.†

The morphology of mLNGs was observed using a JEOL 100 CX transmission electron microscope (TEM), operating at 100 kV. Samples were prepared by diluting latexes at a concentration of 1 mg mL^{-1}. A drop of the diluted latex was placed on copper grids, covered with a film of polyvinyl formal (Sijate®, Fluka), and dried at room temperature. Then, a drop of uranil acetate solution (in a concentration of 1%) was placed on the grids containing the sample and dried again. The micrographs were taken at different magnifications, depending on the particle size.

The minimum film formation temperature (MFFT) of the synthesized latexes was determined employing an optical method,[22] which involved the observation of the clarity of a cast film (120 μm thickness) on a large metal panel. A temperature gradient was applied to the panel and the minimum temperature, where the film was judged to be clear, was considered as the MFFT value.

The internal morphology of the film obtained from mLNGs was studied by TEM. For this, the film was cut using a Leica EM UC6 cryogenic ultramicrotome. A cross-section of the film was deposited on a TEM grid and stained by hydration with one drop of uracil acetate solution at 1%. Upon drying, the sample was observed using a TECNAI G2 20 TWIN microscope (200 kV, LaB6).

The thermal response of films was determined by immersing the sample in deionized water at different temperatures between 20 and 55 °C. At each temperature, the samples were maintained for 30 min to reach the equilibrium, and the absorbed water was determined gravimetrically, by removing the sample from the medium, drying with paper filter, and immediately weighing before immersing again. This procedure was repeated in triplicate.

To determine the ability of mLNGs to load and release a cargo molecule, the protein Ovalbumin (OVA) was used as a model. *In vitro* release studies were carried out on films of 1 cm diameter formed using 45 mg of mLNGs containing 1 mg of OVA. The films were immersed in 2 mL of PBS (pH = 7.4) medium and incubated at 25 °C, in triplicate. At regular intervals, the release medium was replaced, and the amount of released OVA was measured by bicinchoninic acid (BCA) colorimetric assay.

Results and discussion

The designed synthesis strategy reported in this work is pursued for obtaining biphase NGs with multilobular morphology, where the crosslinked PVCL core forms a network that is able to act as a reservoir for cargo molecules and impart thermoresponsive properties to the particle, while the external lobes enable the film forming capability of NGs (Fig. 1). The presence of the external lobes with low T_g in mLNGs is required to promote, during film formation, the polymer diffusion across the interparticle boundary, and hence to produce chain entanglements. This stage is necessary to obtain a cohesive film,[23] which cannot be provided for the PVCL gel phase. When the movement of the

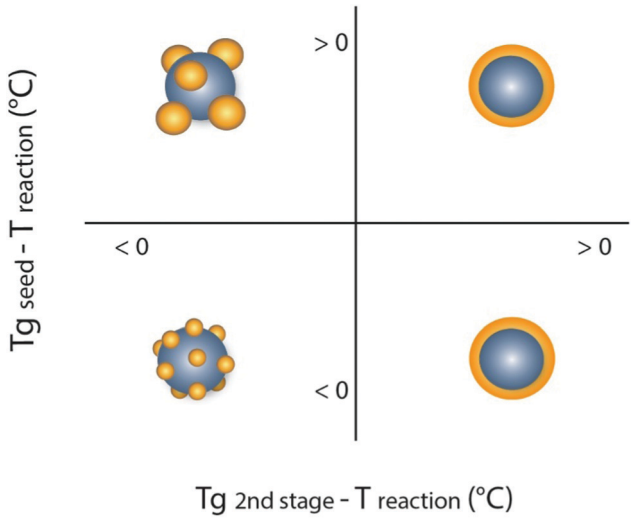

Fig. 3 Simplified diagram of non-equilibrium morphology of particles as a function of T_g of each phase.[25]

phases during synthesis is not hindered and the process is long enough, equilibrium morphologies are governed by the interfacial energy of the system and in the case of particles containing two phases with different degrees of hydrophilicity, the expected equilibrium morphology can be core–shell, inverted core–shell or hemispherical one.[24] Blenner *et al.*[25] studied the key parameters to synthesize nanoparticles with nonequilibrium multilobed morphology by conventional emulsion polymerization and concluded that the key condition is that the second stage oligoradicals in water are not allowed to penetrate significantly to the first stage latex particles and that the seed polymer be more hydrophilic than the second stage polymer. The authors presented a morphology map based on the differences between T_g of the seed ($T_{g,seed}$) and second stage polymer ($T_{g,2nd\ stage}$) with the reaction temperature ($T_{reaction}$). Fig. 3 illustrates the simplified diagram of the resulting morphologies. It should be noted that this analysis does not consider the presence of a crosslinked phase as in the case of the pursued mLNGs, where the generated elastic forces upon the state of deformation within the particle contributes to the resulting morphology.[26,27] However, the crosslinked PVCL phase should not be subjected to significant deformation during particle formation, as a consequence of its high reported T_g (around 200 °C),[4] making the elastic effects negligible.

According to Blenner *et al.*[25] the pursued morphology in this work is a non-equilibrium morphology, because the first stage polymer possesses high T_g and more hydrophilicity (water swellable) phase (PVCL), while the second stage polymer has low T_g and a more hydrophobic phase (poly(VCL-BA)). Since monomers chosen for the synthesis of mLNGs have different reactivities (the reported reactivity ratio of VLC and BA is 0.1 and 1.2,[28] respectively) and water affinities, the simultaneous control of composition and morphology represents a big challenge. Therefore, a synthesis strategy that allows manipulating monomer's availability in the polymerization system will be required. Two mLNGs were synthesized with a semibatch strategy presented in Fig. 2, and the effect of reaction parameters was interpreted in light of a mathematical model for the dynamic development of particle morphology in the second stage of polymerization. Also, a set of sensible properties of the mLNGs were characterized in order to demonstrate the multifunctional performance of these 3-D designed NGs.

Synthesis and characterization of mLNGs

Preparation of mLNGs. Semibatch emulsion copolymerization was carried out following the procedures and reaction parameters displayed in Tables 1 and 2. Fig. 4 shows the global VCL conversion along the semicontinuous reactions and the particle size of NGs measured until the beginning of BA dosification (t_{BA}^{dos}). The overall conversion increased progressively with continuous dosing of VCL. It is worth noting that the first points of overall conversion of VCL are higher than 50% because the initial load of VCL is half of the VCL content of NG formulation. These results indicate that starved conditions are achieved, and VCL is mainly instantaneously consumed and is not accumulated in the polymerization media. BA conversion, as it was expected, was completed along polymerization, since the vinyl bond peaks of unreacted BA were not observed in the samples (Fig. S1 of ESI†).

As it can be observed from Fig. 4, particle sizes of pure VCL NGs, *i.e.* until initiating BA dosification, were around 220 nm for both cases. The size of PVCL NGs is practically equal for both experiments because particle formation is mainly governed by the initial load, which represents half of the total amount of VCL. Although the values of particle size after t_{BA}^{dos} are reported, it is important to note that particles are not spherical, as will be discussed below. Therefore, the diameter

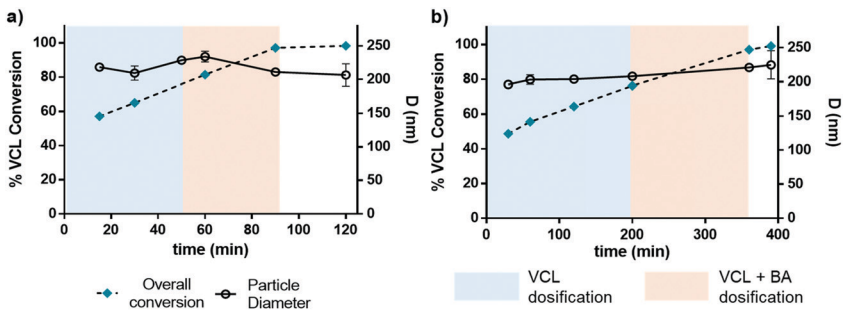

Fig. 4 VCL conversion and D evolution along mLNGs-1 (a) and mLNGs-2 (b) synthesis.

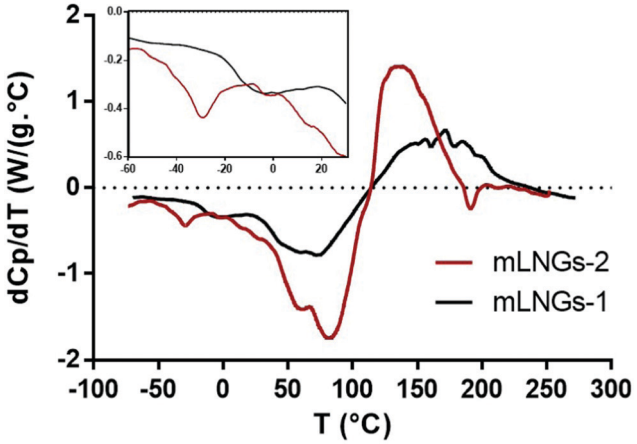

Fig. 5 dDSC thermograms of the first heating cycle of mLNGs-1 and mLNGs-2.

measurements by DLS after t_{BA}^{dos} could be less representative than those measured during the VCL dosing period.

The DSC thermograms reveal the existence of two polymeric phases with very different T_g values in both mLNGs (see for the first cycle in Fig. 5 and for the second cycle in Fig. S2 in the ESI†). In the dDSC thermograms of the second heating cycle, a peak of high temperature around 195 °C is present in both samples (in the first heating cycle, this peak is hindered likely because this phase overlaps with the interphase polymer that shows a broad peak between 30 and 120 °C). This T_g value is close to that reported by Imaz *et al.*[4] for the PVCL NGs with BIS as the crosslinker (200 °C), which resulted in a higher value than the T_g value of the linear PVCL (147 °C)[29] because it was densely crosslinked. This result indicates that the proposed synthesis strategy guarantees the production of a pure crosslinked PVCL phase. Additional peaks are also observed at lower temperatures, which indicated the presence of the poly(VCL-BA) copolymer phase with a lower T_g. The DSC thermograms of the first cycle preserve the information of the morphology of the particles produced in the polymerization[30] and hence their content is more appropriate to determine the composition of the polymeric phases produced during the polymerization reaction. The inset in Fig. 5 shows a zoomed-in view of the peaks corresponding to the low T_g phase for both mLNGs, where it could be observed that T_g of the poly(BA-*co*-VCL) phase was −4.2 °C and −28.5 °C for mLNGs-1 and mLNGs-2, respectively. It is worth mentioning that an ideal random copolymer formed with a VCL/BA ratio equal to 25/75, resulting from the mass dosing ratio of both monomers in both mLNGs, should present a T_g value close to −22.3 °C, calculated by the Flory-Fox equation.[31] This value practically coincides with the T_g observed for the BA-based phase of mLNGs-2, indicating that the reduction of the mass dosing rates led to the formation of the ideal random copolymer with a composition equal to that fed. To understand the composition variation in the low T_g phase of mLNGs, it is necessary to consider the difference in the reactivity ratios between VCL and BA monomers.[28] In this context, when the monomer feeding rates are very low, monomer availability is reduced and true starved conditions are established leading to a copolymer with a composition near the feed composition, as in mLNGs-2 synthesis. On the other hand, by increasing the monomer feeding rates, as in mLNGs-1, a composition drift is generated. Also, the second T_g peak of the BA enriched copolymer of mLNG-2 observed in the second heating cycle of Fig. S2 of the ESI,† could be a consequence of crosslinks formed in the poly(VCL-*co*-BA) phase, where the probability of H abstraction onto polymer BA units is increased with very low monomer availability. It is expected that the presence of a low T_g phase in both synthesized mLNGs should promote the film formation ability of this nanostructured system.

Morphology. In agreement with the DSC results, where transitions corresponding to two phases were found, TEM images confirmed a multilobular morphology in both mLNGs (Fig. 6). Aqueous uranyl acetate solution employed for staining allows differentiating the PVCL core from the poly(VCL-*co*-BA) phase. The crosslinked PVCL is swollen with staining agent solution and uranyl is retained inside its structure after drying. On the other hand, the poly(BA-*co*-VCL) phase does not swell and uranyl is simply adsorbed on the surface of the lobes. Therefore, the crosslinked PVCL phase looks darker than the poly(VCL-*co*-BA) phase. As it can be observed, particles formed with the slowest monomer dosage (mLNGs-2, Fig. 6b) presented a smaller number of lobes per particle than those formed with a faster monomer dosage (mLNGs-1, Fig. 6a). Also, for mLNGs-2, the polydispersity in a number of lobes is smaller than mLNGs-1. As it will be explained below, the number of lobes per particle depends on the interplay between the mechanisms of growing, coagulation and nucleation of lobes.

In order to obtain more insight into the formation of mLNGs, the morphology evolution along both reactions was studied. Fig. 7 shows the TEM images of the samples withdrawn at different times during both reactions. NGs progressed from pure PVCL NGs toward heterogeneous particles with multilobes. The first sample was taken exactly few seconds before t_{BA}^{dos}, which corresponds to the moment of starting the dosage of BA. Until that time, the reaction proceeds as a semibatch emulsion polymerization of VCL in the presence of an initial load of the crosslinker BIS. Pristine PVCL NGs apparently presented two phases of different densities, with a lower dense shell that could indicate the presence of PVCL chains with a lower degree of crosslinking than that of the core,

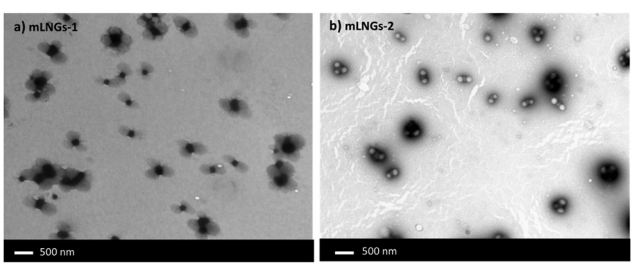

Fig. 6 Final particle morphology of mLNGs-1 (a) and mLNGs-2 (b).

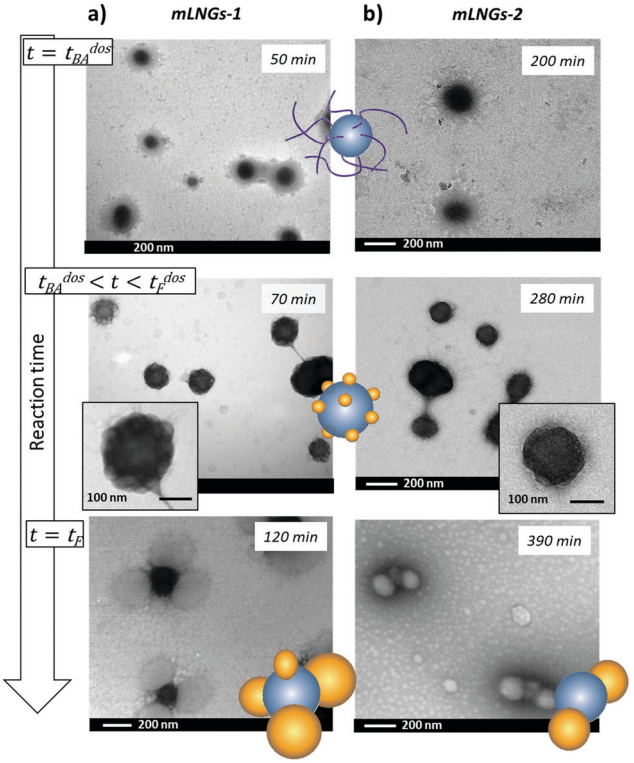

Fig. 7 Particle morphology evolution along mLNGs-1 (a) and mLNGs-2 (b) synthesis.

in agreement with that reported for Imaz *et al.*[4] The second sample corresponds to the middle of the BA feeding period, while the dosage of VCL is maintained. The formation of many small compact lobes (unstained by uranyl agent) on the surface of the pure PVCL NGs was observed (a zoomed-in view of one particle for each intermediate sample is presented in the inset of the corresponding picture). Finally, at the end of the polymerization, NGs presented a shell formed of compact lobes (without staining) of larger size and in lower numbers than those observed in the middle of the dosing BA period (previous sample).

Notably, varying the dosing rate of the monomers generates composite multilobed particles with different numbers of lobes per particle. A previously developed mathematical model[32] is used to study the effect of reaction parameters on the final particle morphology of samples. Here a brief explanation of the model is presented, and for more details, the reader is referred to ref. 20 and 32. The model predicts the dynamic evolution of particle morphology in the second stage of polymerization. In the first stage, which covers from the beginning of the reaction until t_{BA}^{dos}, only VCL and BIS are available in the polymerization media, leading to the formation of a core composed of crosslinked PVCL. These NG particles presented a T_g close to 200 °C, much higher than the reaction temperature (70 °C). Under these conditions, PVCL NG particles act as a seed for the second stage of polymerization. Based on the DSC data obtained, the T_g of the seed was considered as 195 °C and the T_g of the second stage polymer was considered as −4.2 and −28.5 °C for mLNGs-1 and mLNGs-2, respectively.

In the model, the particle morphology is characterized by means of cluster size distributions. The radical concentration profiles were calculated in the model. The profiles were arbitrarily reduced to two regions, one close to the surface and the other representing the rest of the particle as illustrated in Fig. S3 (ESI†). The volume ratio of the regions was considered constant during the process. The model distinguishes between clusters at equilibrium positions and non-equilibrium positions. It is worth mentioning here that the equilibrium morphology of the structured 2 phase polymer–polymer particles in the presence of crosslinked seeds is not yet defined in the literature. Due to the very high T_g and the higher hydrophilicity of the polymer seed as compared with the second stage polymer, the equilibrium morphology was considered as inverted core–shell (the equilibrium position for the second stage polymer, VCL-*co*-BA, was the center of the particle). In addition, the discretization of the radical concentration profile divides the clusters at non-equilibrium into two distributions. Therefore, the particle morphology is characterized by three distributions as illustrated in Fig. S3 (ESI†); the population balances of the non-equilibrium clusters in the exterior region (m1), non-equilibrium clusters in the interior region (m2) and equilibrium clusters at the core of the particles (n). The terms used in the population balances are presented in eqn (S1)–(S14) (ESI†). The values of parameters employed in the mathematical model are given in Table S2 (ESI†).

Fig. 8 shows the model prediction of the final particle morphology as mass cluster distribution of samples mLNGs-1 and mLNGs-2 and their representative TEM-like particles generated from the cluster distributions (see ref. 20 for details on how the TEM-like images are obtained). The high T_g of the seed and high instantaneous conversion during the whole polymerization process led to a very sharp radical concentration profile (see the ESI† for details). As a result of this radical concentration profile, the second stage polymer is formed at the outer

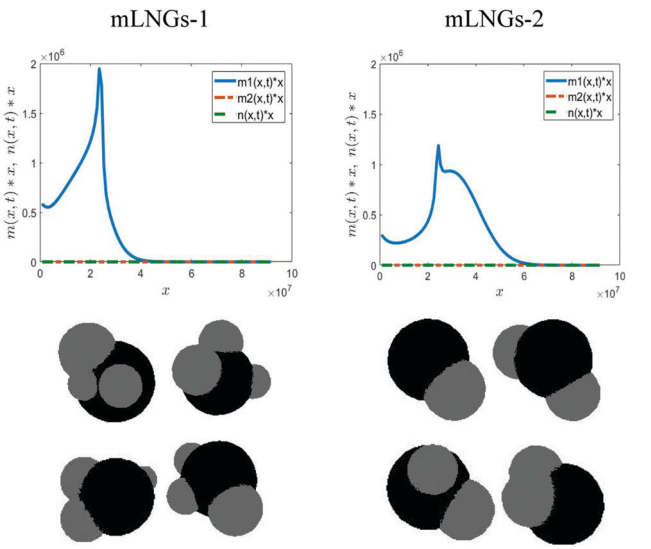

Fig. 8 Predicted mass cluster distributions of samples mLNGs-1 and mLNGs-2 and their representative TEM-like particles.

layer of the particle, which corresponds to the population of the non-equilibrium clusters in the exterior region (m1), and no polymer is formed in the interior zones (m2 and n). On the other hand, due to the high T_g of the seed particles, the movement of the clusters toward the equilibrium position is also hindered. The cluster size distribution of both samples predicted by the model shows that the second stage polymer is only located on the exterior region (m1) and the other two distributions (m2 and n) in the interior zone of the seed particle are equal to zero.

It can be seen that the mass cluster distribution of sample mLNGs-1 shows a narrower distribution indicating a higher number of clusters and smaller ones compared to the mass cluster distribution of the sample mLNGs-2. The average number of lobes per particle predicted by the model is 3.16 and 1.8 for samples mLNGs-1 and mLNGs-2, respectively. This is in reasonable agreement with the experimentally observed particle morphologies in which particles formed with the slowest monomer dosage (mLNGs-2 polymerization, Fig. 6b) presented a smaller number of lobes per particle than those formed with a faster monomer dosage (mLNGs-1 situation, Fig. 6a). While mLNGs-1 has on average 3–4 lobes per particle, most of the particles of mLNGs-2 have just 2 lobes per particle. The size and number of lobes in the exterior zone of the particles are defined by an interplay between the cluster growth (by polymerization and by diffusion of the second stage polymer from the polymer matrix), cluster coagulation and cluster nucleation. A higher rate of polymerization in the sample mLNGs-1 led to a higher rate of nucleation and hence a higher number of nucleated clusters. On the other hand, a softer second stage polymer in sample mLNGs-2 enhanced cluster coagulation that led to a lower number of lobes per particle.

Performance of mLNGs

Thermal response. Fig. 9 shows the thermal response of mLNGs (mLNGs-1 and mLNGs-2), together with pure PVCL NGs used as the reference as the ratio between the swollen diameter D(T) and collapsed diameter (Dc) at 55 °C. PVCL NGs were obtained by semibatch polymerization under the same conditions as mLNGs-1, but without adding BA. Even though the morphology of mLNGs is very far from spherical (especially for mLNGs-2), this comparison allows determining roughly how the presence of hydrophobic lobes in PVCL NGs influences their thermal response. As could be observed, the thermal response of mLNGs is not affected by the presence of shell lobes, with the transition temperature being approximately 32.5 °C for both cases. Notably, the swelling capacity of mLNGs (between 1.9 and 2.5) is reduced when compared with that of pure PVCL NGs (3.0), likely because more than 50% of mLNGs are composed of lobes that do not swell. Moreover, the measured swelling capacity of mLNGs is in agreement with the reported ranges for PVCL NGs (around 2.2).[4]

Film properties. Beyond the difference in their morphologies, both mLNGs were able to form films, with an MFFT lower than 7 °C (the minimum temperature measured with the equipment) which indicates that they are able to form films at room temperature. In order to study the internal structure of the film, a cross-section of films obtained with both mLNGs was observed by TEM, (Fig. 10). Dark zones observed in Fig. 10a, which correspond to the PVCL core, are surrounded by lighter particles of the poly(VCL-*co*-BA) phase and exactly reflected the morphology of mLNGs-1. On the other hand, in Fig. 10b, both phases are distributed almost alternately, in agreement with the observed particle morphology for mLNG-2. In both films, the morphology of mLNGs is preserved and the limits of lobe particles are well defined, indicating an incomplete particle inter-diffusion. The presence of this particular internal film morphology, where lobes are not completely coalesced, is desirable because the presence of pores in the formed film facilitates the mass transfer from the PVCL phase to the media (a required film capability during swelling and delivering of a cargo molecule).

In Fig. 11a, the water uptake of films at 25 °C is plotted, where the mLNGs-2 film presented a higher swelling degree compared to mLNGs-1. This result could be a consequence of the lower number of lobes per particle, which enables further expansion of the crosslinked PVCL core phase of mLNGs. Despite this difference in swelling capacity, both films have a very similar thermal response (Fig. 11b), being swollen at low temperatures and collapsing at temperatures above body

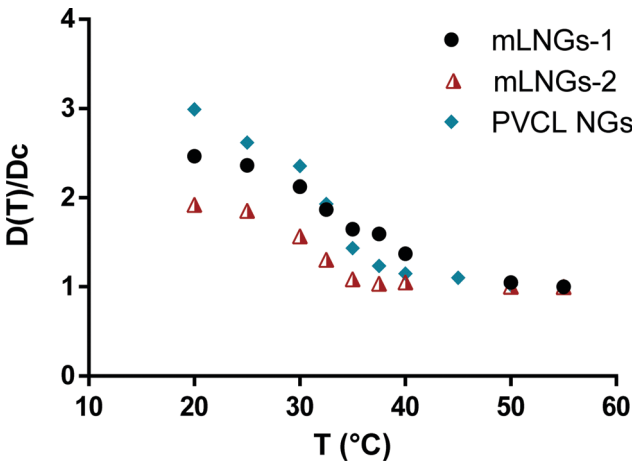

Fig. 9 Thermal response of both mLNGs and pure PVCL NGs as the ratio of swollen diameter, $D(T)$ and collapsed diameter at 55 °C (Dc).

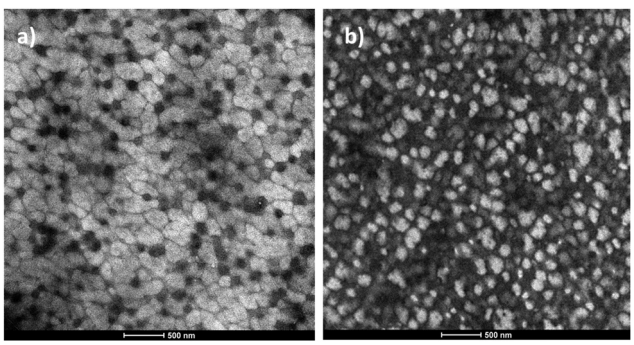

Fig. 10 TEM micrograph of the morphology of the cross-section of the mLNGs-1 (a) and mLNGs-2 (b) films.

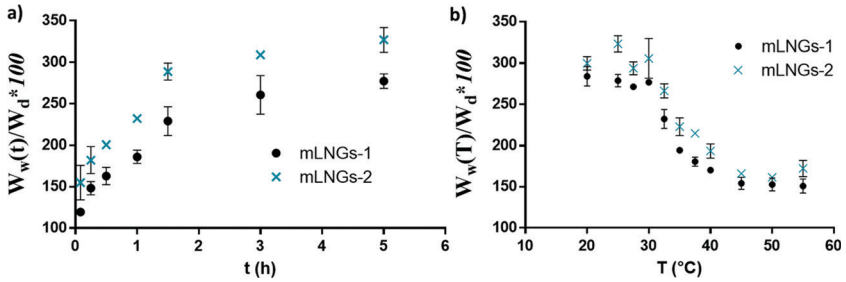

Fig. 11 Water uptake at 25 °C (a) and thermal response (b) of both mLNG films, expressed as a weight ratio between the wet film sample (W_w) and the dried state (W_d).

temperature, with a very similar transition. Note that both samples presented a water gain of around 50% when they are in the collapsed state (55 °C), while their maximum swelling reached at 20 °C was around 300%.

Protein controlled release. Finally, the ability of mLNGs to load and release a model protein (ovalbumin, OVA) was evaluated. 0.54 mL of both mLNG dispersions (83 mg mL^{-1}) were loaded with 1 mg of OVA and film discs of 1 cm of diameter were formed by casting. Fig. 12 shows the OVA release profile as the cumulative percentage of OVA released with respect to the loaded OVA. It can be seen that OVA release from mLNGs-2 is faster than from mLNGs-1. This observation could be a consequence of the particular morphology of mLNGs, where the presence of lobes has an impact on the releasing area of the PVCL core and could contribute to retaining and delaying the protein delivery. In that sense, in a film formed with NGs with a lower amount of lobes per particle, as in mLNGs-2 sample, a faster OVA release is observed. In the same way, the higher swelling capacity observed in mLNGs-2, Fig. 11a, also contributes to extending the releasing area, favoring the OVA release. This trend is in agreement with that reported by Bettini *et al.*,[33] where the influence of releasing area on drug delivery was studied by partially coating hydrogels with an impermeable film. The power-law equation of Korsmeyer–Peppas, previously used for thermoresponsive NG drug release (eqn (S21) of the ESI†),[34] was used to model the obtained OVA release profile. According to this equation, the drug release mechanism is modelled by the diffusion exponent '*n*', where it occurs by either Fickian diffusion when $n < 0.43$, or by Anomalous (non-Fickian) diffusion if $0.43 < n < 0.89$, or by case-II transport when $n = 0.89$ or by Supercase-II transport when $n > 0.89$.[35] Table S4 of the ESI,† summarizes the values of *n* and the correlation coefficients (R^2) for both mLNGs. It can be seen that in both systems, OVA release is nearly governed by a Fickian diffusion (n = 0.44 and 0.49 for mLNGs-1 and mLNGs-2, respectively), indicating that it is mainly modulated by the protein diffusion throughout the polymer matrix of the mLNG film. Finally, the results obtained in this section evidence that the release of a cargo molecule could be tuned by varying the number of lobes per particle in mLNGs, expanding the potential of mLNGs as a delivery platform.

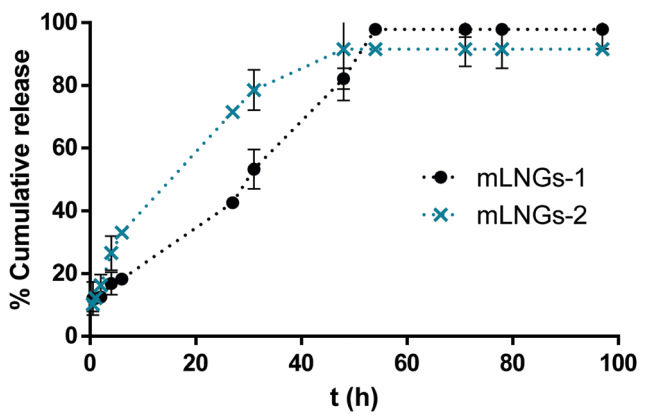

Fig. 12 OVA release in PBS from mLNGs-1 and mLNGs-2 (n = 3, mean ± SD).

Conclusion

Novel multilobed biphase NGs composed of a crosslinked PVCL core and poly(VCL-*co*-BA) lobes were successfully synthesized. The employed synthesis strategy involved one-pot semibatch polymerization, where adequate manipulation of monomer feeding streams allowed the production of the PVCL core first and subsequently the formation of a shell of poly(VCL-*co*-BA)-based lobes. This proposed synthesis procedure has been demonstrated to be able to synthesize mLNGs containing variable compositions and lobes by just changing the monomer feeding rates. Specifically, when monomer feed rates were drastically reduced, the mLNGs passed from having an average of 3–4 lobes per particle to just 2 softer lobes per NGs. These results were in reasonable agreement with those obtained from a previously developed mathematical model, which predicts the dynamic evolution of particle morphology during the second stage of polymerization, where the mLNGs are formed. Simulation revealed that high monomer feeding rates led to a higher rate of cluster nucleation and hence to a higher number of lobes per NGs. On the other hand, the softer second stage polymer formed with slower monomer feeding rates enhanced cluster coagulation and the particles presented a lower number of lobes.

These synthesized mLNGs showed a multifunctional functionality as a result of the synergy between the contribution of both the core and lobe phases and their key morphological arrangement. While the PVCL-based core conferred the

characteristic thermal response and the ability to load and release a cargo molecule, the low T_g of poly(VCL-*co*-BA)-based external lobes incorporated the capability of coalescence (*i.e.*, film forming). Also, the multilobular arrangement of NGs allowed the formed films to undergo unrestricted mass transfer from the PVLC core and the delivery medium. Films formed from mLNGs showed a thermal response around body temperature and they were able to deliver a model protein, with a quite retarded releasing rate when the number of lobes per NGs was increased. The distinguished multifunctional performance of mLNGs makes them a good candidate for their application in wound dressing, transdermal vaccination or drug delivery, where the occlusion effect produced by the film may enhance the skin permeability of the therapeutic cargo molecules.

These results indicate that the proposed synthetic method allows extending the properties and the application of NGs, by opening new horizons to explore novel combinations of polymeric phases and obtaining innovative synergetic functionalities.

Author contributions

A. S. Sonzogni: investigation, data curation, and writing – original draft preparation; S. Hamzehlou: methodology, formal analysis, and writing – review & editing; V. D. G. Gonzalez: writing – review & editing; J. R. Leiza: funding acquisition, and writing-review & editing; R. J. Minari: conceptualization, project administration, funding acquisition, supervision, and writing – review & editing.

Conflicts of interest

There are no conflicts to declare.

Acknowledgements

The authors acknowledge the financial support from the Argentinean Government (PIP 1122015 0100231-CO and PICT-2016-3876), the Universidad Nacional del Litoral (C. A. I. + D 50420150100100LI), the Basque Government (GC-IT-999-16), and MINECO (CTQ2017-87841-R). The authors are also grateful to SGIKER (TEM Analysis Services from UPV/EHU) and its technicians Ana Martinez and Maite Miranda for the TEM characterization. S. Hamzehlou thanks the University of the Basque Country (UPV/EHU) for the ''Contratación para la especialización de personal investigador doctor'' postdoctoral grant.

References

1 N. Tiwari, A. S. Sonzogni and M. Calderón, *Nanomedicine*, 2019, **14**, 2891–2895.
2 M. Giulbudagian, M. Asadian-Birjand, D. Steinhilber, K. Achazi, M. Molinaa and M. Caldero, *Polym. Chem.*, 2014, **5**, 6909–6913.
3 A. Imaz and J. Forcada, *Macromol. Symp.*, 2009, **281**, 85–88.
4 A. Imaz and J. Forcada, *J. Polym. Sci., Part A: Polym. Chem.*, 2008, **46**, 2510–2524.
5 J. Ramos, A. Imaz and J. Forcada, *Polym. Chem.*, 2012, **3**, 852–856.
6 M. Molina, M. Giulbudagian and M. Calderón, *Macromol. Chem. Phys.*, 2014, **215**, 2414–2419.
7 J. C. Cuggino, C. I. Alvarez, M. C. Strumia, P. Welker, K. Licha, D. Steinhilber, R. C. Mutihac and M. Calderón, *Soft Matter*, 2011, **7**, 11259–11266.
8 A. Imaz and J. Forcada, *J. Polym. Sci., Part A: Polym. Chem.*, 2010, **48**, 1173–1181.
9 F. Meeussen, *Polymer*, 2000, **41**, 8597–8602.
10 A. Imaz and J. Forcada, *J. Polym. Sci., Part A: Polym. Chem.*, 2008, **46**, 2766–2775.
11 A. Imaz, J. I. Miranda, J. Ramos and J. Forcada, *Eur. Polym. J.*, 2008, **44**, 4002–4011.
12 A. Imaz and J. Forcada, *Eur. Polym. J.*, 2009, **45**, 3164–3175.
13 W. Sun, S. Thies, J. Zhang, C. Peng, G. Tang, M. Shen, A. Pich and X. Shi, *ACS Appl. Mater. Interfaces*, 2017, **9**, 3411–3418.
14 J. Siirilä, M. Karesoja, P. Pulkkinen, J. M. Malho and H. Tenhu, *Eur. Polym. J.*, 2019, **115**, 59–69.
15 A. Imaz and J. Forcada, *J. Polym. Sci., Part A: Polym. Chem.*, 2011, **49**, 3218–3227.
16 G. Aguirre, J. Ramos and J. Forcada, *Soft Matter*, 2013, **9**, 261–270.
17 F. Xu, J. Zhu, L. Lin, C. Zhang, W. Sun, Y. Fan, F. Yin, J. C. M. van Hest, H. Wang, L. Du and X. Shi, *Theranostics*, 2020, **10**, 4349–4358.
18 J. G. Tsavalas, F. J. Schork and K. Landfester, *Journal of Coatings Technology and Research*, Springer, New York LLC, 2004, vol. 1, pp. 53–63.
19 S. Hamzehlou and J. R. Leiza, *Advances in Polymer Science*, Springer, New York LLC, 2018, vol. 281, pp. 105–141.
20 S. Hamzehlou, J. R. Leiza and J. M. Asua, *Chem. Eng. J.*, 2016, **304**, 655–666.
21 A. S. Sonzogni, G. Yealland, M. Kar, S. Wedepohl, L. M. Gugliotta, V. D. G. Gonzalez, S. Hedtrich, M. Calderón and R. J. Minari, *Biomacromolecules*, 2018, **19**, 4607–4616.
22 J. L. Keddie, *Mater. Sci. Eng., R*, 1997, **21**, 101–170.
23 M. A. Winnik, *Curr. Opin. Colloid Interface Sci.*, 1997, **2**, 192–199.
24 L. J. Gonzalez-Ortiz and J. M. Asua, *Macromolecules*, 1995, **28**, 3135–3145.
25 D. Blenner, J. Stubbs and D. Sundberg, *Polymer*, 2017, **114**, 54–63.
26 Y. G. Durant, E. J. Sundberg and D. C. Sundberg, *Macromolecules*, 1996, **29**, 8466–8472.
27 Y. G. Durant, E. J. Sundberg and D. C. Sundberg, *Macromolecules*, 1997, **30**, 1028–1032.
28 S. Verbrugghe, K. Bernaerts and F. E. Du Prez, *Macromol. Chem. Phys.*, 2003, **204**, 1217–1225.
29 N. A. Cortez-Lemus and A. Licea-Claverie, *Prog. Polym. Sci.*, 2016, **53**, 1–51.
30 A. K. Tripathi, J. G. Tsavalas and D. C. Sundberg, *Thermochim. Acta*, 2013, **568**, 20–30.
31 T. G. Fox and S. Loshaek, *J. Polym. Sci.*, 1955, **15**, 371–390.

32 N. Rajabalinia, *Precise Characterization and Modeling of Particle Morphology Development in Emulsion Polymerization*, University of Basque Country (UPV/EHU), 2019.
33 R. Bettini, P. Colombo, G. Massimo, P. L. Catellani and T. Vitali, *Eur. J. Pharm. Sci.*, 1994, **2**, 213–219.
34 Q. Wang, Y. Zhao, Y. Yang, H. Xu and X. Yang, *Colloid Polym. Sci.*, 2007, **285**, 515–521.
35 E. Ortiz-Islas, A. Sosa-Arróniz, M. E. Manríquez-Ramírez, C. E. Rodríguez-Pérez, F. Tzompantzi and J. M. Padilla, *Rev. Adv. Mater. Sci.*, 2021, **60**, 25–37.

